

# **Modeling of Continuous-Casting Defects Related to Mold Fluid Flow**

Brian G. Thomas  
Department of Mechanical and Industrial Engineering  
140 Mech. Engr. Bldg., MC-244, 1206 W. Green St.  
Univ. of Illinois at Urbana-Champaign  
Urbana, IL61801, U.S.A.  
Tel: 217-333-6919, Fax: 217-244-6534  
bgthomas@uiuc.edu

**Keywords:** Continuous Casting, Submerged Entry Nozzle, Mold Flow, Gas Injection, Air Aspiration, Level Fluctuations, Inclusion Entrapment, Meniscus Hooks, Surface Defects, Slag Entrainment, Computational Fluid Dynamics, Models, Solidification

## **ABSTRACT**

The quality of continuous-cast steel is greatly influenced by fluid flow in the mold, particularly at the meniscus. Recent examples of computational model applications at the University of Illinois are presented to investigate the formation of several different types of defects related to flow phenomena. The amount of gas injection into the tundish nozzle to avoid air aspiration is quantified by modeling. Computational model calculations of superheat transport and surface level fluctuations are presented. Meniscus defects, such as subsurface hooks and their associated inclusions, may form if the superheat contained in the steel is too low, or if top-surface level fluctuations are too large. A thermal stress model has been used to compute the distortion of the meniscus during a level fluctuation. Gas bubbles and inclusion particles may enter the mold with the steel flowing through the submerged nozzle. In addition, mold slag may be entrained from the top surface. These particles may be removed safely into the slag layer, or may become entrapped into the solidifying shell, to form sliver or blister defects in the rolled product. Transient, turbulent flow models have been applied to simulate the transport and entrapment of particles from both of these sources. The insights gained by these modeling efforts aid greatly in the development of processing conditions to avoid the formation of these defects.

## **INTRODUCTION**

In the continuous casting of steel, the task of the flow system is to transport molten steel at a desired flow rate from the ladle into the mold cavity and to deliver steel to the meniscus area that is neither too cold nor too turbulent. In addition, the flow conditions should minimize exposure to air, avoid the entrainment of slag or other foreign material, aid in the removal of inclusions into the slag layer and encourage uniform solidification. Achieving these somewhat contradictory tasks needs careful optimization.

Fluid flow in the mold is controlled by many design parameters and operating conditions. Nozzle geometry is the most important, and includes the bore size, port angle, port opening size, nozzle wall thickness, port shape (round, oval, square), number of ports (bifurcated or multiport), and nozzle bottom design). The flow pattern also depends on parameters which generally cannot be adjusted to accommodate the flow pattern, such as the position of the flow control device (slide gate or stopper rod), nozzle clogging, casting speed, strand width, and strand thickness. Fortunately, other parameters besides nozzle geometry can be adjusted to maintain an optimal flow pattern. These include the injection of argon gas, nozzle submergence depth, and the application of electromagnetic forces. In choosing optimal settings for these parameters, it is important to understand how they all act together to determine the flow characteristics. An increase in casting speed, for example, might be compensated by a simultaneous increase in submergence depth (or electromagnetic force), in order to maintain the same surface flow intensity. Thus, all of the flow-control parameters must be optimized together as a system.

In designing the flow system, it is important to consider transients. Sudden changes are the main cause of the flow instabilities which generate surface turbulence and other problems. Because flow parameters are more easily optimized only for steady operation, each of the parameters which affects fluid flow must be carefully controlled. It is especially important to keep nearly constant the liquid steel level in the mold, powder feeding rate (to keep a constant liquid slag layer thickness), casting speed, gas injection rate, slide gate

opening, and nozzle position (alignment and submergence). It is also important to choose flow conditions which are resistant to transients and their detrimental effects, although this is difficult to predict.

Many quality problems that originate during the continuous casting of steel can be directly attributed to poor control of fluid flow conditions in the mold <sup>[1]</sup>. In order to optimize these flow design and operation conditions, it is crucially important to understand how defects arise, and how they are affected by changes in the flow pattern affect those defects. This paper summarizes some of these problems and illustrates the use of computational flow models in gaining insight into them, using recent examples developed through the Continuous Casting Consortium at the University of Illinois.

## DEFECTS RELATED TO FLUID FLOW

A schematic of the continuous casting process is given in **Fig. 1**, which illustrates some of the phenomena which lead to defects due to fluid flow in mold region of the process. Jets of molten steel are directed into the liquid by the nozzle ports and traverse across the mold cavity to impinge on the solidifying steel shell near the narrow faces. Gas bubbles in the jet lower its density, providing lift which may alter the flow pattern. The jets impinging against the narrow face may cause shell thinning, and even breakouts, if the superheat is too high and the interfacial gap is excessive <sup>[2]</sup>. The momentum of the upward flow along the narrow faces can raise the meniscus level there, causing a nonlinear profile along the top surface. Where this level is too high, the infiltration of liquid mold flux into the interfacial gap becomes more difficult, which can lead to nonuniform meniscus heat flux, longitudinal cracks, and other surface defects.

Excessive surface turbulence may cause rapid fluctuations of the surface level. This can disrupt stable solidification at the meniscus, leading to deep oscillation marks, surface depressions, surface cracks, and local entrapment of mold slag leading to delamination defects. In addition, high speed flow across the top surface may shear droplets of liquid mold slag into the flow, where they may become entrained in the liquid steel.

On the other hand, if the surface velocities are insufficient, or if the local superheat contained in the molten steel near the meniscus is too low, then the meniscus may partially freeze to form deep oscillation marks and meniscus “hooks”. These hooks are detrimental because they may entrap particles into the solidifying meniscus. Superheat also affects the nucleation and growth of equiaxed grains, which controls the solidification structure, and defects such as centerline segregation. The transport of solute with the fluid is also of crucial importance to macrosegregation problems, especially towards the final solidification point lower in the strand.

In addition to steel and superheat, the jets carry bubbles and inclusion particles into the mold cavity. If the flow pattern enables the particles to reach the top surface, they should be harmlessly removed into the liquid slag layer, so long as the slag is not saturated and the surface tension forces are not excessive. Alternatively, inclusions and bubbles may become entrapped into the solidifying steel shell, where they cause slivers, “pencil-pipe” blisters, and other costly defects. Inclusion particle behavior is complicated by their attachment to the surface of bubbles, which encourages removal, but also creates potentially-dangerous large clusters, which may also be created through collisions.

## COMPUTATIONAL MODELING OF FLUID FLOW

### Governing Equations

Computational models to simulate fluid flow phenomena in three dimensions generally start by solving the continuity equation and Navier-Stokes equations for incompressible Newtonian fluids, which are based on conserving mass (one equation) and momentum (three equations) at every point in a computational domain. This yields the pressure and velocity components at every point in the domain. The domain is discretized into small computational cells which should exactly match the true shape of the flow region of the process, in this case the nozzle and liquid pool of the continuous casting mold and upper strand. When this is performed with a sufficiently-refined grid to directly capture the details of the transient fluid flow pattern, this is called “direct numerical simulation”. Because this generally leads to excessive execution times, the computational grid is generally coarsened, and a “subgrid model” is

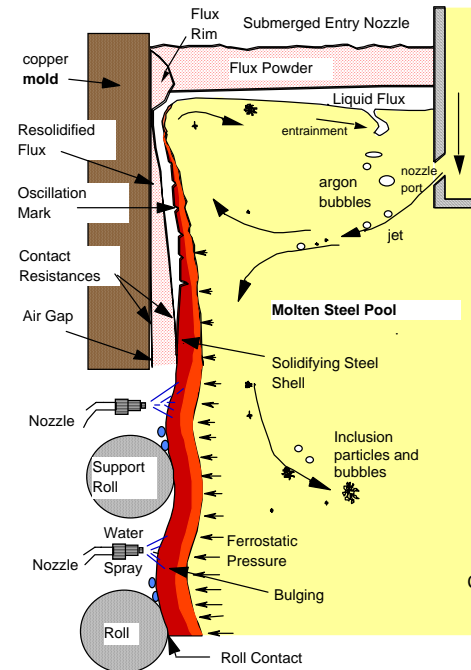


**Fig. 1.** Flow Phenomena in the continuous-casting mold region

used to account for the effects of turbulence which occur at time and length scales smaller than an individual computational volume. This paper contains many examples using this method, which is called “Large Eddy Simulation”<sup>[3, 4]</sup>. To achieve even more efficient computation on coarse grids or meshes, the effects of turbulence can be treated as an artificial increase in the fluid viscosity, which is determined by solving additional transport equations for the time-averaged flow pattern. The most popular of these Reynolds-Averaged Navier Stokes or “RANS” methods is the  $k-\epsilon$  turbulence model, which solves two additional transport equations for the turbulent kinetic energy,  $k$ , and its dissipation,  $\epsilon$ <sup>[5]</sup>. The relative advantages and accuracies of these approaches for continuous casting are compared elsewhere<sup>[5, 6]</sup>.

Unless solidification is modeled together with the flow, then the shape of the liquid domain must be obtained through other means (such as a heat conduction model of shell solidification – CON1D<sup>[7]</sup>). In addition, flow through the boundaries of this domain must be imposed to satisfy the solidification rate, by specifying fixed velocity boundary conditions at the walls, as explained elsewhere<sup>[3, 8]</sup>. When coarse-grid RANS models are used, the thin boundary layer of the liquid is smaller than the computational cells at the walls, so are taken into account using “turbulent wall functions”,<sup>[6]</sup>.

To obtain accurate flow solutions, it is often necessary to couple the flow equations together with simultaneous solution of other equations, in order to incorporate other phenomena<sup>[9]</sup> such as gas injection, or electromagnetic stirring / braking. For example, when a significant amount of gas is injected with the steel, its buoyancy requires a multiphase model. Many different computational approaches are possible to simulate this behavior<sup>[9]</sup>. Ultimately, it is of crucial importance to validate the flow model predictions through comparison with measurements as much as possible, such as PIV measurements in water models<sup>[10]</sup>.

### Mold Geometry and Casting Conditions Studied

To illustrate the application of some of these models to understand continuous casting defects, examples are taken from simulations conducted at the University of Illinois. For simplicity, almost all of the examples involve the same thin-slab caster using the domain in **Fig. 2**. The tapered nozzle has two 15°-down 75x32mm ports and a third round port directed straight downward, and has 127mm submergence. The straight-walled mold cavity and upper strand is 132mm thick by 984mm wide, cast at 1.5m/min with 58 °C of superheat, 434 stainless steel and no gas injection. Further details are given elsewhere on the casting conditions<sup>[11]</sup>, computational model equations<sup>[3, 12]</sup>, and experimental measurements<sup>[11, 12]</sup>.

An example of the fluid flow velocities in the nozzle and mold region of this thin-slab continuous caster are presented in **Fig. 3**<sup>[3]</sup>. Note the significant asymmetry in the instantaneous flow pattern in the nozzle, both around the stopper rod, Fig. 3 a) and at the nozzle ports, Fig. 3 b). Flow varies chaotically between sides, in spite of the perfectly symmetrical domain, and long time operation, reaching a “pseudo-steady” state. This continues into the mold region, as Fig. 3c) shows differences from the time average, Fig. 3d). Generally, this example is a reasonably-stable classic double-roll flow pattern. Flow impinges on the narrow faces, splits upward and downward, and traverses the top surface back towards the SEN.

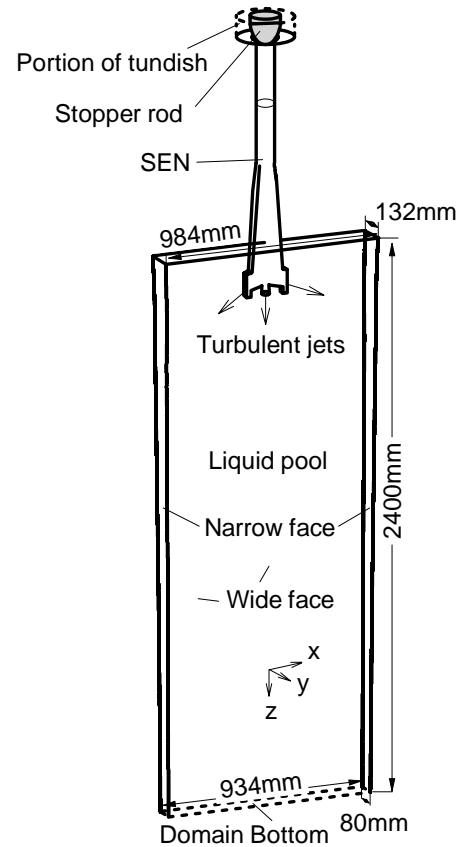


**Fig. 2.** Schematic of the computational domain of the thin-slab steel caster, including tundish nozzle<sup>[3]</sup>.

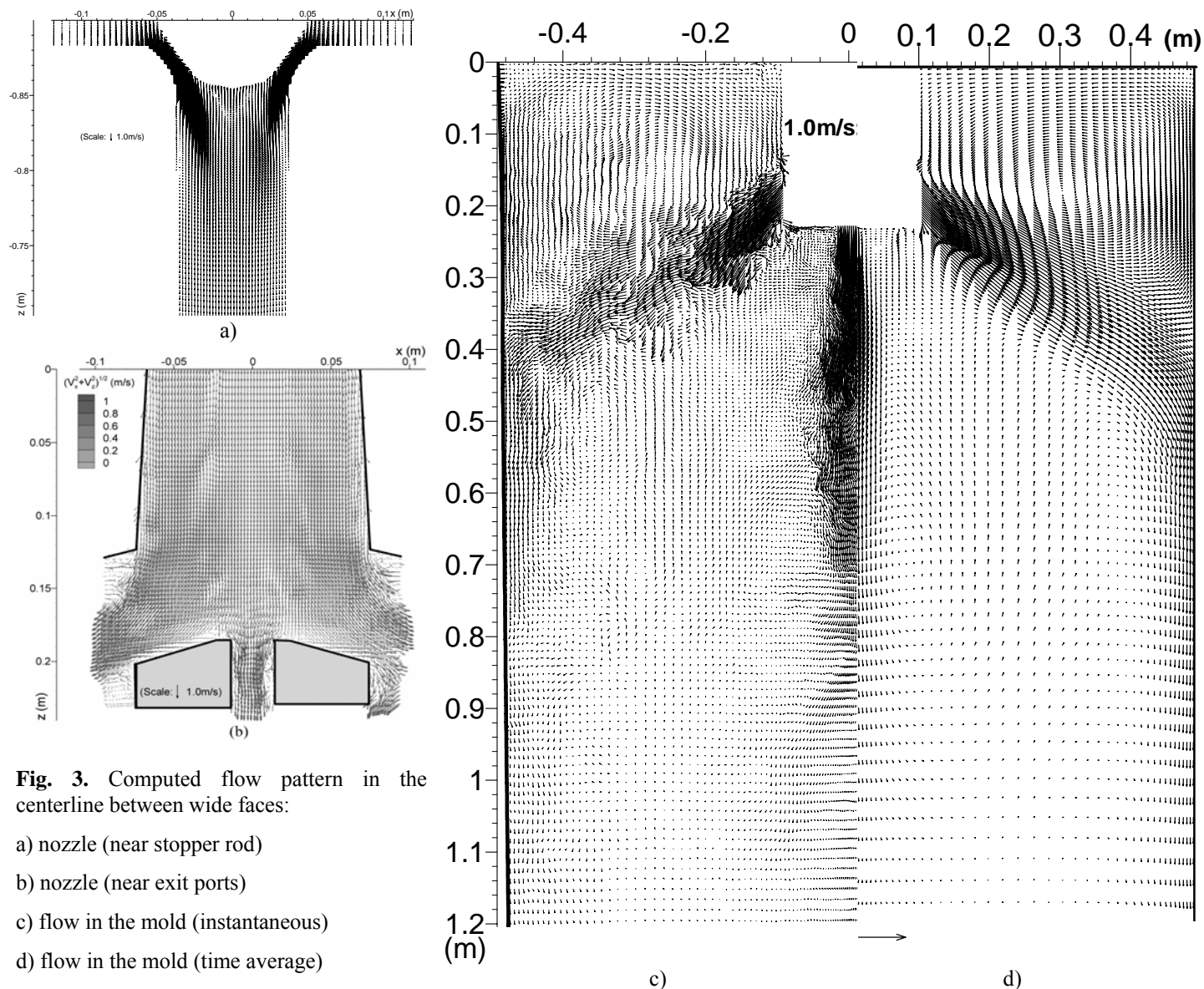


**Fig. 3.** Computed flow pattern in the centerline between wide faces:

- a) nozzle (near stopper rod)
- b) nozzle (near exit ports)
- c) flow in the mold (instantaneous)
- d) flow in the mold (time average)

### MODELING OF PHENOMENA RELATED TO DEFECTS

Although it is a challenging task to compute, it must be remembered that the average flow pattern itself is of no practical interest! Rather, it is a necessary first step in the simulation of related phenomena, which depend on the fluid flow and cause defects in the steel product. With the tremendous increases in computing power and modeling sophistication, computational models are becoming increasingly able to simulate these important related phenomena.

One important phenomenon is the effect of argon gas injection on the pressure distribution, buoyancy, direction, and pattern of the fluid flow, in both the nozzle<sup>[13-15]</sup> and mold<sup>[16, 17]</sup>. The transport of superheat with the flow<sup>[18]</sup>, and solidification of the steel shell<sup>[7, 19]</sup>, are important phenomena to meniscus hook formation, shell thinning, breakouts, internal microstructure, and macrosegregation. Solute transport governs intermixing during grade changes<sup>[20, 21]</sup> and also affects segregation. Inclusion particle transport with the flow directly controls cleanliness of the product<sup>[22]</sup>. Particles in the flow are subject to many forces, especially in the boundary layers near the solidification front, and at the slag-metal interface<sup>[12]</sup>, which govern entrapment of the particles into the solidification front. A new entrapment criterion has recently been developed and is presented elsewhere in these proceedings<sup>[12]</sup>. Other important phenomena include bulging (for the liquid pool shape changes which affect segregation) and metallurgical thermodynamics (which affects inclusion precipitation, nozzle clogging, and solidification microstructure). Finally, the model must be applied in parametric studies to learn something useful about the real process.

## AIR ENTRAINMENT DEFECTS

Exposure to air at any stage after steel refining leads to detrimental oxide inclusions in the steel product. This problem is worst at the final stage of flow in the mold, because there is little opportunity to prevent the reoxidation products from becoming entrapped in the final product as catastrophic large inclusions.

Open stream pouring produces the worst air entrainment problems, which is the reason for submerged entry nozzles and mold flux operation. Air entrainment is still possible, however, if there are leaks, cracks, inadequate sealing between the nozzle joints or if the nozzle material becomes porous. If the internal pressure in the nozzle drops below atmospheric pressure, air tends to aspirate through these pathways into the nozzle. This can be identified by nitrogen pickup, and dendritic inclusions from reaction in a high oxygen environment. Pressure in the nozzle is lowest just below the flow control device, due to the venturi effect of the metal stream. For a given steel flow rate, the pressure drop (and corresponding tundish height) both increase as the opening area is restricted, as shown in **Figs. 4** and **5** for a typical slide gate nozzle <sup>[15]</sup>. The results in these figures were computed using a 3-D multiphase flow of a typical bifurcated nozzle with 15° downward 78mm square ports <sup>[15]</sup>. The Eulerian-Eulerian model solves two complete sets of mass and momentum balance equations for the gas and liquid phases, which are fully coupled together through the phase fractions. The model was run many times with varying argon injection rate under feasible conditions (ie varying slide gate opening and casting speed together appropriately for a given tundish depth).

Air aspiration into the nozzle can be discouraged by proper introduction of an inert gas flow, which is one of the ways in which argon gas acts to prevent nozzle clogging. Adding argon gas can replace air in feeding leaks around seals. Argon injection also can raise the minimum pressure in the nozzle above ambient <sup>[15]</sup>. Note that this occurs because the slide gate must open up to accommodate the gas (shown in the top of Fig. 5), in addition to the pressurizing effect of the gas. The minimum gas flow rate calculated to avoid a partial vacuum is shown in Fig. 5 (bottom). When the slide gate opening is either very small or very large, the pressure never drops below one atmosphere (zero gage pressure), so gas injection is not needed to prevent aspiration. Less gas is needed at low casting speed and at low tundish level, when the pressure drops are lower. Maintaining a high gas flow rate during these times may disrupt flow in the mold and thereby be detrimental to steel quality.

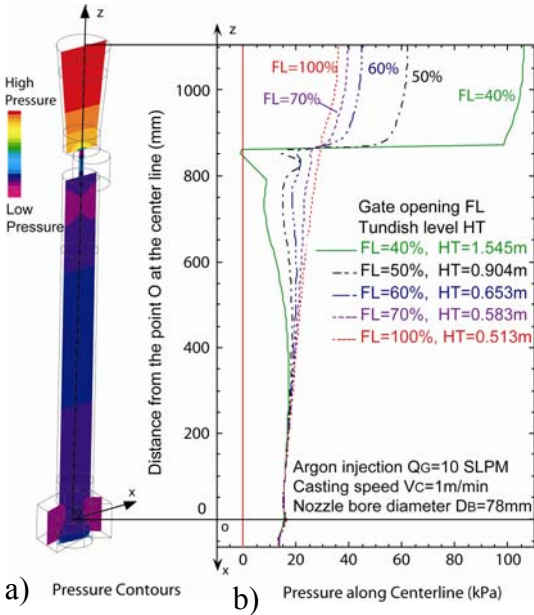


**Fig. 4.** Pressure drop calculated down nozzle <sup>[23]</sup>  
a) Pressure contours in centerplane showing that major variations are in vertical direction  
b) Effect of slide gate opening on vertical pressure distribution

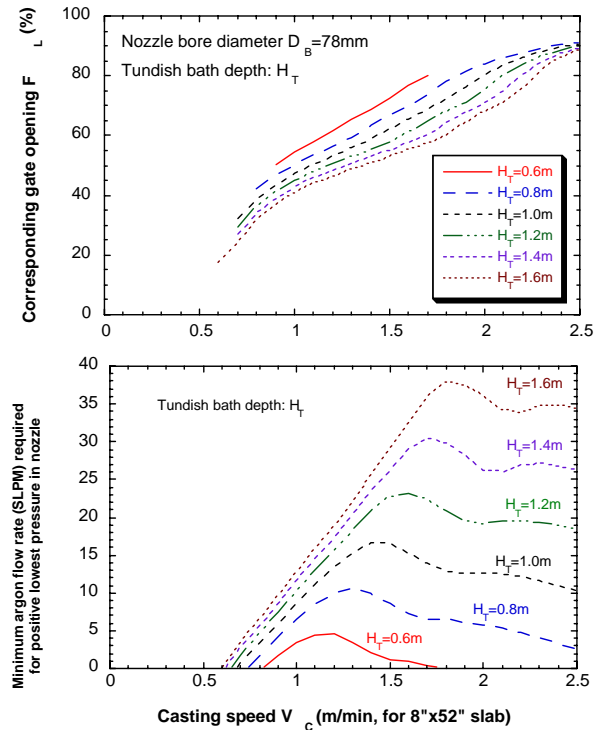


**Fig. 5.** Optimizing argon gas injection (for a 78-mm bore nozzle with 90° slide-gate) <sup>[23]</sup>

## SUPERHEAT TRANSPORT, SHELL THINNING, AND BREAKOUTS

Impingement of the molten steel jets onto the solidifying shell in the mold can cause problems if the jet is either too hot or too cold. Breakouts occur when the steel shell at mold exit is not strong enough to contain the liquid steel and have many causes. One possible cause is local thin and hot regions of the solidifying shell, which can result from high superheat dissipation at the region where an excessively hot jet impinges on the inside of the shell<sup>[18, 24]</sup>. Problems arise only if this local superheat dissipation is combined with slow heat extraction from the corresponding shell exterior. This problem is most likely in the off-corner regions, where the jet may impinge and the shell shrinkage also creates a larger gap.

A computational model of superheat transport has been developed for the 132mm thin slab caster in Fig. 2<sup>[6, 25]</sup>. This computation is challenging because the thermal boundary layer has steep gradients, especially in the critical impingement region, which requires a very fine grid. The temperature contours presented in **Fig. 6** reveal the temperature distribution in various horizontal sections. The jet leaving the nozzle ports is hottest, and quickly dissipates its superheat and drops in temperature as it moves through the mold. Measurements of temperature from a probe inserted down into the top surface (**Fig. 8**) agree with the predictions that roughly 70% of the superheat is gone at this location, which provides partial validation of the model. The predicted temperature fluctuations, indicated with the error bars, also bracket the variation in the probe measurements. Most (65%) of the superheat is dissipated to the shell in the mold (**Fig. 7**) with most of the remainder dissipated just below mold exit<sup>[25]</sup>. As is common in slab casting with bifurcated nozzles, the impingement region on the narrow face absorbs the most superheat (12%), and has double the average heat flux per unit area to the wide face. Each wide faces removes 26% of the superheat, but its area is over 7X larger. This high-impact region on the narrow face extends to the off-corner region of the wide faces. Heat losses through the top slag layer are small.

**Figure 9** shows how shell growth depends on the combined effects of superheat input from jet impingement and heat removal to the mold walls<sup>[26]</sup>. Model predictions were made using a comprehensive heat-flow solidification model of the mold, interface, and shell, CON1D, which features momentum, mass, and force (friction) balances on the liquid flux layer<sup>[7, 19]</sup>. Jet impingement produces a thinner shell on the narrow face, compared with classic parabolic shell growth on the wide face, as shown in both the computations and measurements in **Fig. 9**<sup>[26]</sup>. The importance of this shell-thinning effect increases with higher casting speeds, higher superheats, and lower gap heat transfer<sup>[18, 24]</sup>. Asymmetric flow, such as caused by nozzle clogging may aggravate the effect.

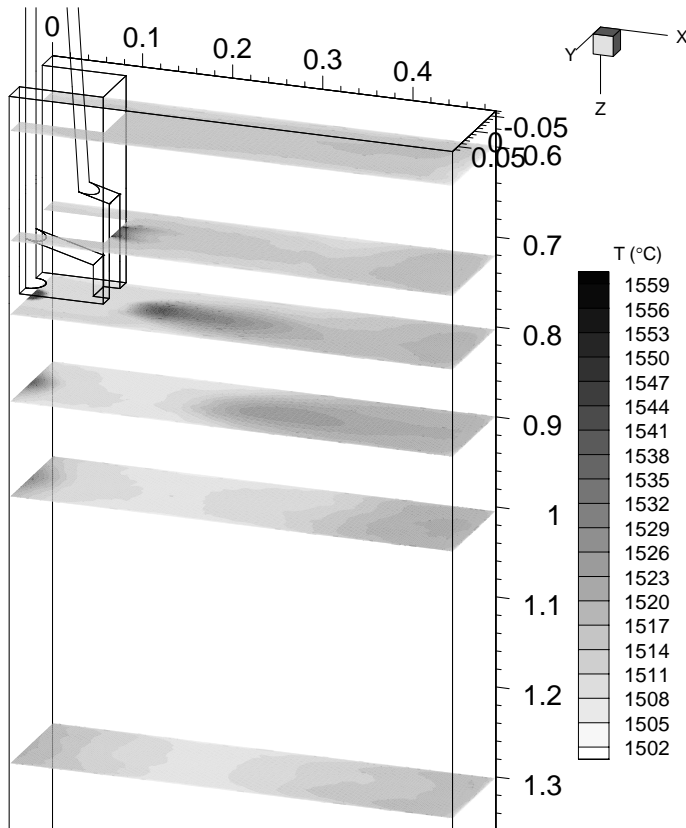


**Fig. 6.** Temperature distribution in liquid pool (based on flow conditions in Fig. 3)<sup>[25]</sup>

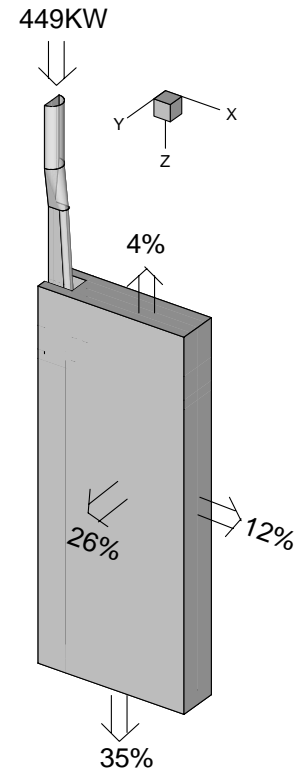


**Fig. 7.** Superheat removal distribution (based on temperatures in Fig. 6)<sup>[25]</sup>

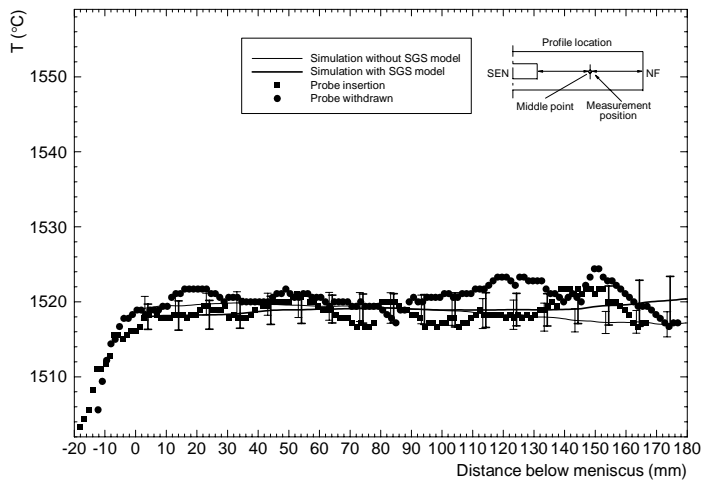


**Fig. 8.** Comparison of simulated temperature profile and plant measurements (#3 – 295mm from CL) <sup>[17, 25]</sup>

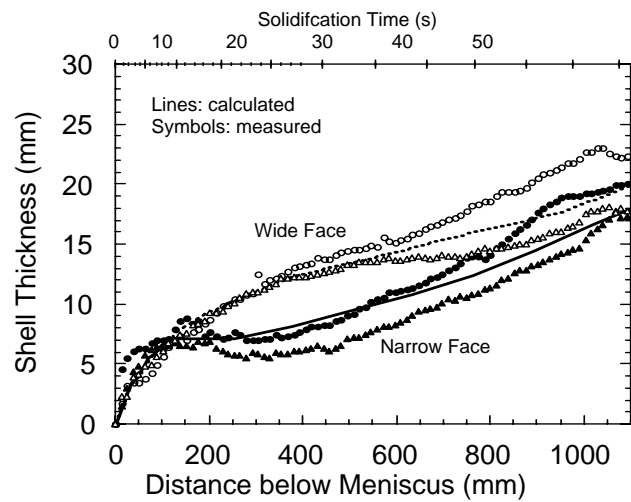


**Fig. 9.** Breakout shell thickness profiles and corresponding model predictions, showing thin region near location of jet impingement on narrow face, relative to steady shell growth down wide face <sup>[26]</sup>.

## SURFACE DEFECT FORMATION

Most surface defects in the steel product originate in the mold at the meniscus, where the solidifying steel shell is very thin. The most obvious source of surface defects is the capture of foreign particles into the solidifying shell at the meniscus. Particles come from many sources, including argon bubbles, oxide inclusions generated by prior processes that are carried in with the steel entering the mold cavity, and slag entrainment. If they are not removed by scale formation or during scarfing, these surface inclusions will lead to line defects or “slivers” in the final product. Other problems include deep oscillation marks and surface depressions, which lower the local heat transfer, leading to a hotter local shell temperature, strain concentration, and crack formation. Transverse cracks often form during unbending at the root of the deep oscillation marks. Longitudinal cracks often initiate at local hot spots around the meniscus perimeter. All of these defects are worsened by large fluctuations in the top surface liquid level, which depend on the flow pattern in the mold.

Many surface defects form at the meniscus due to variations in the level of the liquid steel on the top surface of the mold cavity. These variations take two forms: a relatively steady contour across the mold width known as a “standing wave”, and “level fluctuations”, where the local level changes with time. While the standing wave can cause chronic problems with liquid slag feeding, the time varying level fluctuations cause the most serious surface defects.

### Top Surface Level Profile

The top-surface level is important because it affects the feeding of liquid flux into the interfacial gap between the mold and shell, which is important to heat transfer. Insufficient liquid flux consumption to the interfacial gap leads to increased thermal resistance, variable heat transfer, thermal stresses, stress concentration, and ultimately, cracks. A steep surface level profile makes it difficult for complete coverage of the liquid flux over the steel surface. If the liquid flux layer becomes so thin that the steel surface touches the mold powder, it can become contaminated with elements such as carbon, which can cause surface quality problems such as cracks and segregation in ultra-low carbon steels.

**Figure 10** shows a typical instantaneous profile of the transient top surface level obtained from the flow field in Fig. 3 <sup>[3, 27]</sup>. This computation was achieved by performing a balance between kinetic energy and potential energy on the results of pressure along the top surface. The predictions in a water model prediction compared well with measured top surface levels <sup>[3]</sup>. The results in Fig. 10 also compare with measurements of the top surface level in the steel caster, obtained by dipping thin steel sheets. The results match within the uncertainty in the measurements (error bars), which exists regarding possible rotation of the sheets. The level is always higher near the narrowfaces, by 2mm in the water model and 4-6mm in the steel caster. This is because the steel upward momentum near the narrowfaces lifts the liquid level there, displacing some of the molten flux. The flux layer must be thick enough to cover the steel, in order to provide a steady supply of molten flux into the interfacial gap to lubricate the steel. Thus, the height of the surface “standing wave” is important to steel quality.

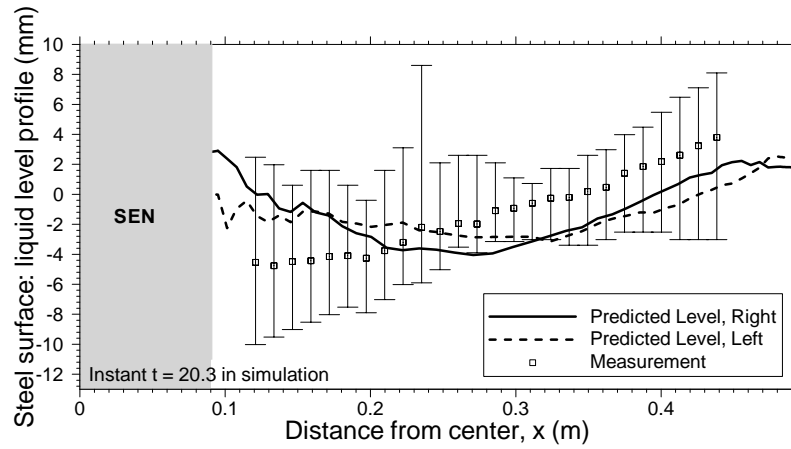


**Fig. 10.** Comparison of predicted and measured top surface liquid levels in steel (Fig. 3 flow field) <sup>[3]</sup>.

### Top Surface Level Fluctuations

Controlled oscillation of the mold generates ripples across the liquid level, but does not present an inherent quality problem, because the liquid near to the mold wall tends to move with the wall. Large, sudden jumps or dips in liquid level are much more serious.

A sudden jump in local level can cause molten steel to overflow the meniscus. In the worst case, the steel can stick to the mold wall and start a sticker breakout. Alternatively, a jump in level can cause an irregular extended frozen meniscus shape, or “hook”. This defect is discussed in the next section. Variations of more than the oscillation stroke over a time interval on the order of one second are the most detrimental. Even low frequency variations (period >60s) may cause defects, if the meniscus overflows and the solid slag rim is imprinted on the shell or captured <sup>[28]</sup>.

A sudden severe drop in liquid level exposes the inside of the solidifying shell to the mold slag, and also leads to surface depressions. Relaxing the temperature gradient causes cooling and bending of the top of the shell toward the liquid steel. When the liquid level rises back, the solidification of new hot solid against this cool solid surface layer leads to even more bending and stresses when the surface layer reheats <sup>[29]</sup>. This sequence of events is illustrated on a 20mm long section of shell in the thermal-stress model results in **Fig. 11**, for a 20-30mm level drop lasting 0.6s <sup>[29]</sup>. When liquid steel finally overflows the meniscus to continue with ordinary solidification, a surface depression is left behind, such as shown in Fig. 11.

The microstructural changes and surface depressions associated with level variations are serious because they initiate other quality problems in the final product. These problems include surface cracks and segregation. Surface cracks allow air to penetrate beneath the steel surface where it forms iron oxide, leading to line defects in the final product. These defects are difficult to distinguish from inclusion-related defects, other than by the simpler composition of their oxides.

**Figure 12** shows the time-variation of the horizontal velocity towards the SEN at the center points between the SEN and the narrowface on the top surface. This result was obtained from the transient Large Eddy simulation <sup>[3]</sup>. The velocity fluctuations are very large – similar to the velocity magnitude. Figure 12 shows a strong component with high frequency (e.g. flow velocity drops from ~0.4m/s towards the SEN to a velocity in the opposite direction within 0.2s).

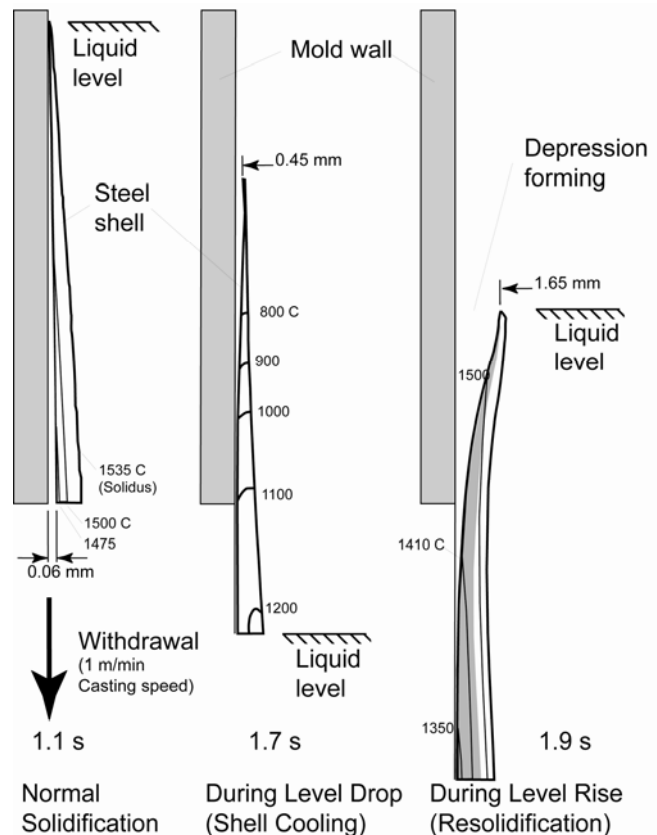


**Fig. 11.** Events during a severe, level drop (20 mm for 0.6 sec) which lead to a transverse surface depression <sup>[29]</sup>



This prediction compares favorably with previous PIV measurements on a 0.4-scale water model <sup>[10]</sup>. Simulations with and without flow across the centerline reveal that interaction between the two sides of the caster is an important cause of the large high frequency fluctuations. This agrees with findings based on water modeling <sup>[30]</sup>. These velocity variations are significant, because the level fluctuations which accompany them are a major cause of defects in the process. This is revealed in time-dependent animations of the profile in Fig. 10 <sup>[3]</sup>.

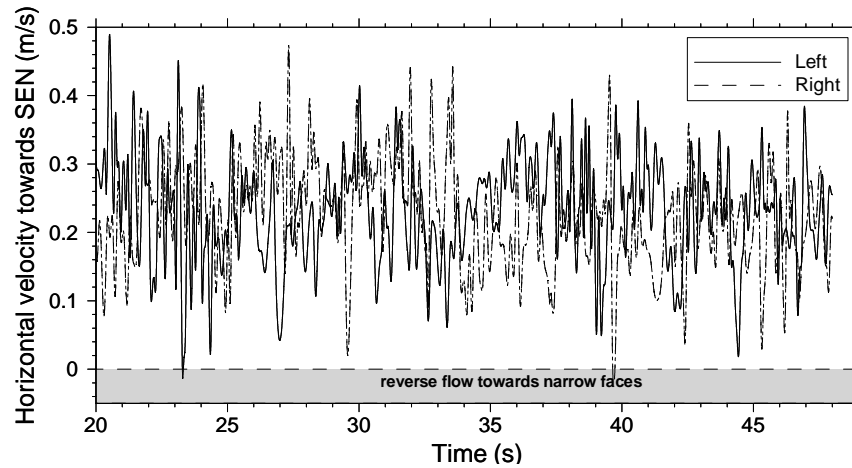


**Fig. 12.** Time variations of the horizontal velocity towards SEN at the center point of the top surface of steel (see Figs. 2 and 3)

### Surface Hook formation

Subsurface hook formation at the meniscus during the continuous casting of steel slabs is an important cause of surface defects, owing to their easy entrapment of mold flux and inclusion-laden gas bubbles. **Figure 14** shows a typical hook, which is usually associated with an oscillation mark and especially plagues ultra-low carbon steels <sup>[31, 32]</sup>. Their formation mechanism is not completely understood, owing to the complexity of phenomena at the meniscus, and the difficulty of obtaining good measurements. They are known, however, to be affected by steel grade, superheat, level fluctuations, and oscillation conditions <sup>[31, 32]</sup>.

The effect of superheat is investigated by close examination of the superheat results, shown in Fig. 6 <sup>[25]</sup>, and further application of computational models to the meniscus region. As the steel flows through the mold cavity, it continuously drops in temperature. The coldest liquid is found at the meniscus, around the perimeter of the top surface, especially near the narrow face and the wideface centerline near the inlet nozzle. The fluid is coldest here because it is both far from the inlet and stagnant. In extreme cases, these regions are subject to meniscus freezing, skull formation, and even “bridging”, where steel or slag freezes across the shortest distance between the nozzle and meniscus of the wide face, often leading to a breakout.

The heat flux corresponding to superheat delivery to the solidifying steel shell in the critical meniscus region is shown in **Fig. 13** (for slightly different casting conditions chosen to match the hook in Fig. 14 <sup>[33]</sup>). The lowest superheat flux is found at the corner and near the nozzle, which coincides with the locations where the deepest meniscus hooks are observed in practice. Hooks also tend to be deeper on wide slabs with low superheat and low casting speed, for the same reasons.

Using a best estimate for superheat flux at the meniscus, the solidification of the initial shell was computed with CON1D, and the thickness compared with the measured hook shell thickness in Fig. 14 <sup>[32]</sup>. For the calculation, the meniscus location where the hook shell starts is taken at one theoretical oscillation mark pitch above the measured deepest part of the oscillation mark at the hook. This suggests that the etched hook shape was created by a change in heat flow conditions that occurred due to metal overflow of the initial shell at the meniscus at the instant that the oscillation mark formed. The predicted shell profile roughly matches the measured profile. The results suggest that the top of the actual hook shell was truncated, likely due to breaking-off or melting during the liquid overflow event. Further computational efforts are currently being conducted to investigate the fundamental formation mechanism of these hooks.

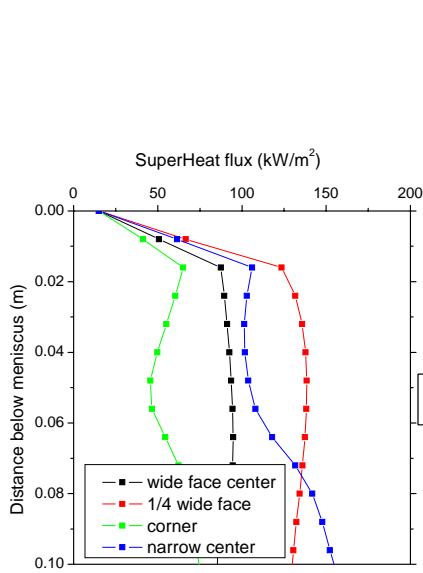


**Fig. 13** Variation of superheat flux in meniscus region around strand perimeter <sup>[33]</sup>

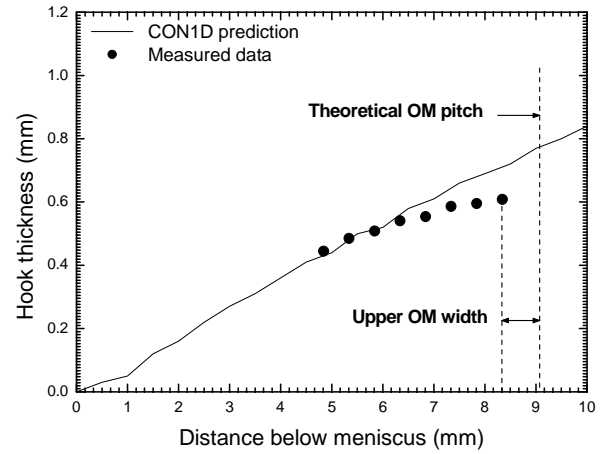
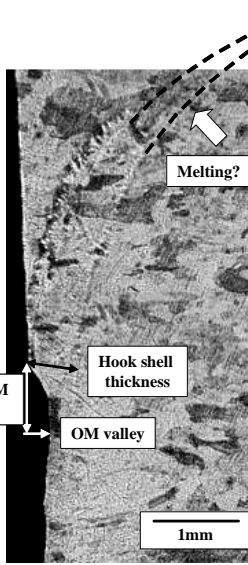


**Fig. 14.** Typical hook shape (left) and comparison of hook-shell thickness with shell thickness prediction from CON1D <sup>[32]</sup>

### INCLUSION PARTICLE ENTRAPMENT

The entrapment of inclusions, bubbles, slag, and other particles during solidification of steel products is a critically-important quality concern. They require expensive inspection, surface grinding and even rejection of the final product. Furthermore, if undetected, large particles lower the fatigue life, while captured bubbles and inclusion clusters cause slivers, blisters, and other surface defects in rolled products. These particles have two main sources: bubbles and inclusions generated during upstream processing which enter the mold through the submerged entry nozzle, and the entrainment of mold slag from the top surface, discussed in the next section.

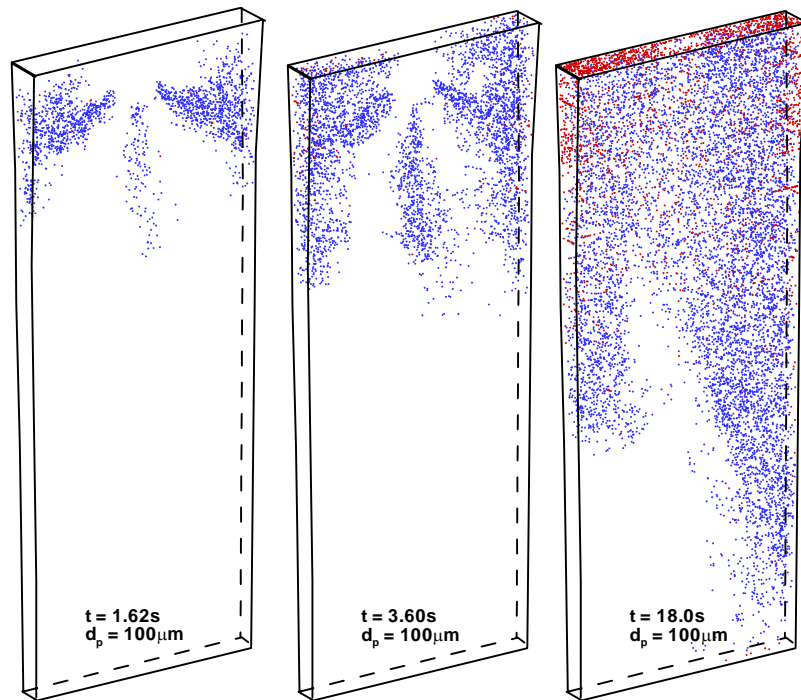


**Fig.15.** Transport of 100  $\mu\text{m}$  inclusions in strand at different times (red = final entrapment location, based on flow pattern in Fig. 3) <sup>[4]</sup>

Particles leaving the tundish can either stick to the nozzle walls, where they lead to clogging, travel with the recirculating flow to be safely removed into the mold slag at the top surface, or become entrapped into the solidifying shell, where they lead to product defects. The fraction of particles going to each of these destinations is being quantified using a new computational model. This model first calculates the transient turbulent flow field in the mold region using Large Eddy Simulation (LES), with a sub-grid-scale (SGS)  $k$  model <sup>[3]</sup>. Next, the transport and capture of many individual particles are simulated using a Lagrangian approach to track the trajectories <sup>[4]</sup>. The results presented here are for 30,000 particles, in order to achieve reasonable statistics. The transport equation includes the effects of six hydrodynamic forces: drag, shear-lift, pressure-gradient, stress-gradient, added-mass, Basset history, and buoyancy. The model features a new criterion to determine particle entrapment, which considers the effects of four more forces which are important in the fluid boundary layer adjacent to the solidification front. Further details on the model are given in the other paper <sup>[12]</sup> and elsewhere <sup>[8]</sup>.

Instantaneous snapshots of the trajectories of 100  $\mu\text{m}$  alumina inclusion particles at different times after entering in the mold region are shown in **Fig. 15**, based on the flow pattern in Fig. 3.

Note that the domain includes the 1.11m submerged entry nozzle and the top 2.40m of the steel strand. Particles which touch the top surface are assumed to be removed into the slag layer (and are then colored red). Note that significant asymmetry exists in the flow, which directly affects the particles, especially in the lower regions of the strand. Many more particles leave from the right side of the domain, although investigation revealed that there was no significant asymmetry at the nozzle port exit. This behavior is attributed solely to the chaotic nature of turbulence.

### Nozzle Entrapment (Clogging)

The inclusion trajectories themselves are of much less practical interest than their final entrapment locations. Inclusions attaching to the nozzle walls contribute to clogging, which is detrimental to steel quality in several ways: the clogging slows production; large clogs can suddenly break off and enter the mold; and the flow pattern becomes unstable<sup>[15]</sup>.

An example of the predicted locations of inclusions touching the nozzle walls are shown in **Fig. 16**. About 10% of the particles exiting the tundish touched the stopper rod, and a further 16% touched an inner wall of the nozzle<sup>[8]</sup>. These inclusions might stick to cause nozzle clogging in a real caster, depending on the properties of the nozzle material and thermodynamic reactions at the interface. Note that the bottom portion of the stopper rod and nearby walls of the upper nozzle have the most inclusion entrapment, which agrees with plant experience. Some particles touched the bottom of the SEN near the outlet ports.

### Strand Entrapment (Sliver Defects and Blisters)

Particles traveling in the liquid pool may become entrapped into the solidifying shell to form defects. In the new entrapment criterion, particles touching the solidification front were assumed always to become entrapped if they are smaller than the primary dendrite arm spacing. Larger particles are subjected to a force balance which considers the effects of transverse fluid flow on washing the particles away from the interface, the angle of the reaction forces between the dendrite tips, and the other hydrodynamic forces. In addition, this force balance includes the effects of the surface tension gradient, such as caused by sulfur rejection at the solidification front, the lubrication force, and Van-der-Waals forces. All three of these forces tend to encourage particle entrapment, and should be explored in further work. Further details on the entrapment criterion are given in the other paper<sup>[12]</sup>.

Inclusion entrapment locations in the final solidified strand were computed from the trajectory results, shown in Fig. 15, and are presented in **Fig. 17**. Over 84% of the 100  $\mu\text{m}$  inclusions were captured in the shell, including 51% in the upper 2.4m of the strand. Only 8% touched the top slag surface, while the remaining 8% touched the outside of the nozzle refractory walls and might be removed. After injecting larger 400  $\mu\text{m}$  inclusions, only 30% were entrapped in the solidified shell. This is due both to their increased chances of flotation from their higher buoyancy, and to their smaller likelihood of capture into the solidification front.

The particles were injected through the nozzle ports during a 9s time period, which corresponds to 0.23m of travel of the meniscus down with the strand, and is labeled on Fig. 17. The entrapment locations in the strand are distributed both upstream and downstream about this location. The side and top views, Figs. 17 a) and b), show that the captured particles concentrate in a thin band around the strand perimeter, and especially near the narrow faces. There does not appear to be any significant concentration of particles associated with flow from the central port. Fig. 17d) reveals strong asymmetry in the particle trajectories through the liquid, as many more particles exit the left side of the domain into the lower strand. However, this asymmetry appears to be greatly diminished in the final entrapment locations, as Fig. 17c) shows much less bias towards the left side. This is because faster moving flow across the solidification front makes capture more difficult. Capture is most likely along those regions of flow along the solidification front which move slowly downward near the casting speed. It is important to emphasize that the asymmetry is chaotic and although the stronger flow to the left persisted for a long time interval, (>30s), it could change to the opposite side at any time.

By reprocessing the results to model continuous inclusion injection, it is possible to compute the expected distribution of total oxygen content in an average section through the final solid strand<sup>[4]</sup>. **Figure 18** presents the results for 10 ppm total oxygen content entering from the nozzle ports in the form of 100  $\mu\text{m}$  particles. Figure 18 shows that the entrapment is concentrated from 10-25mm beneath the strand surface at the centerline. Considering the shell thickness profile down the strand, this region corresponds to a capture

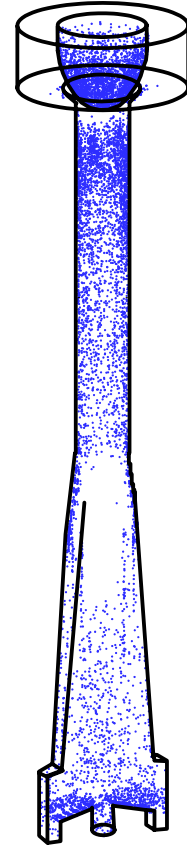


**Fig. 16** Final Entrapment location of inclusions on stopper rod and nozzle walls (flow conditions in Fig. 3)

region of  $\sim 0.5\text{--}2.5$  m below the meniscus. Local spikes in total oxygen in this band depend on sample size, but are predicted to exceed 60ppm, owing to grouping together of captured particles simply due to chaotic turbulence. The final entrapment position in the lower strand is uncertain, so this region is represented as a dashed line. Its average oxygen content is 6ppm, indicating that relatively fewer particles penetrate deeper than 2.5m below the meniscus into the lower regions of the strand.

The caster simulated here has straight vertical walls. In a curved caster, large particles in the lower recirculation zone tend to spiral towards the inner radius, with increased entrapment rates. Entrapped solid oxide particles eventually lead to surface slivers or internal defects, which act as stress concentration sites to reduce fatigue and toughness properties of the final product. Gas bubbles captured in this way eventually may cause blister defects such as “pencil pipe” which appear as streaks in the final rolled product. When the slab is rolled, the subsurface bubbles elongate and the layer of metal separating them from the surface becomes thinner. Later during annealing, they can expand to raise the surface of the sheet locally, especially if the steel is weak such as ultra-low carbon grades, or if hydrogen is present<sup>[34]</sup>. Further computations are needed to quantify the expected benefits of lowering the casting speed, or using a vertical mold and upper strand.

These results suggest that most of inclusions which enter the mold become entrapped in the final product. Thus, nozzle design and mold operation should focus on controlling flow at the meniscus to avoid the further entrainment of new inclusions, rather than altering the flow pattern to encourage the removal of inclusions entering the mold. Upstream operations should focus on inclusion removal and reoxidation prevention.

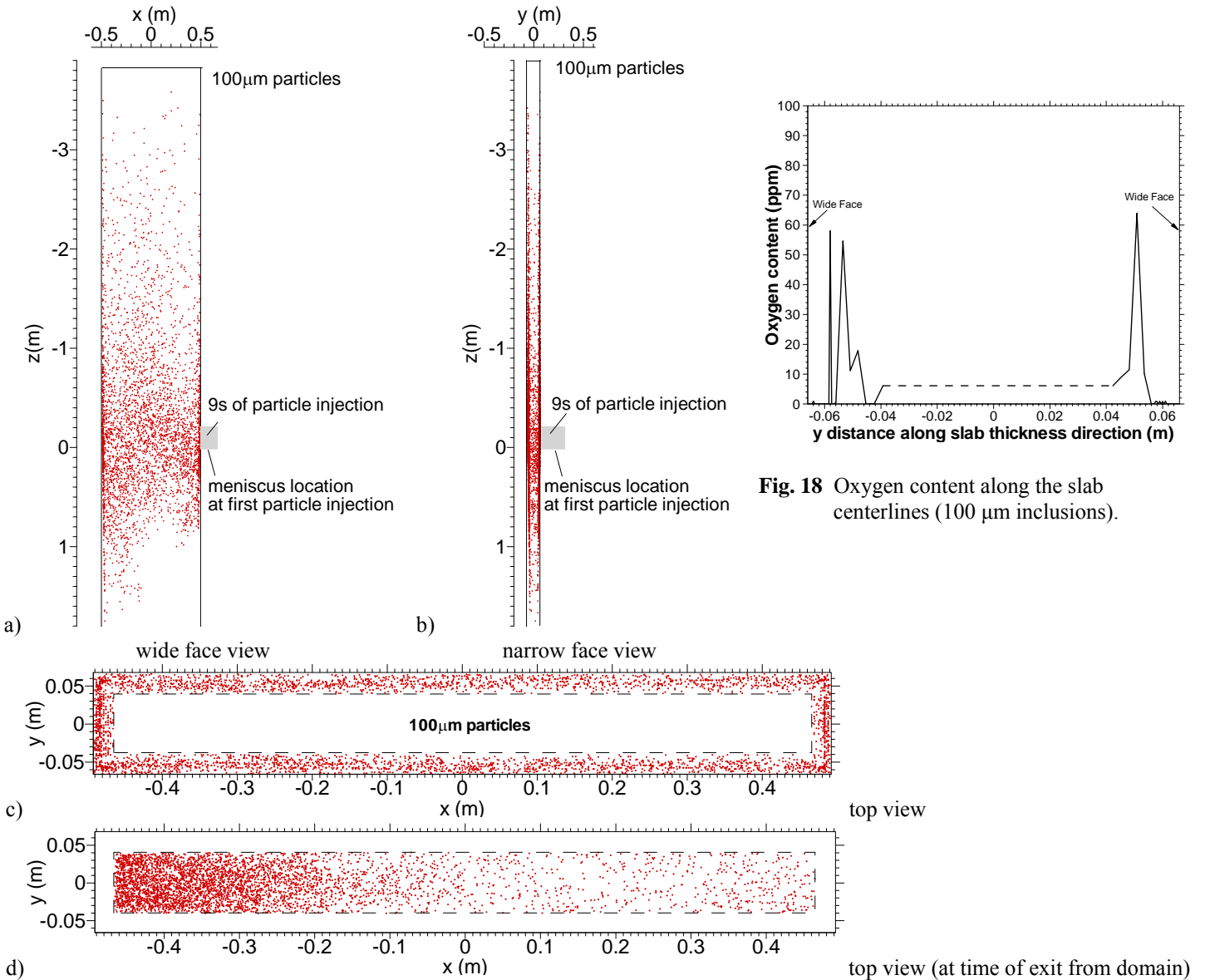


**Fig. 17.** Particle entrapment locations predicted in the final solidified strand (based on trajectories in Fig. 15)

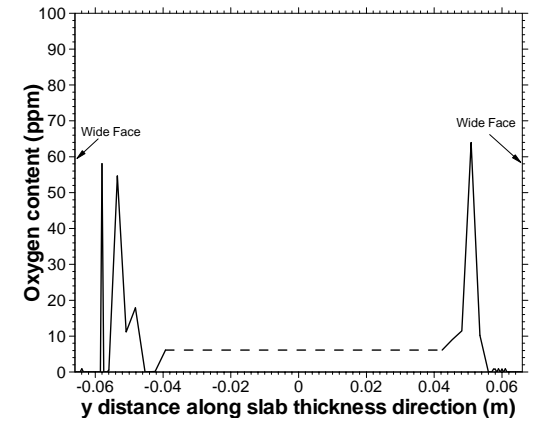


**Fig. 18** Oxygen content along the slab centerlines (100 μm inclusions).

## MOLD SLAG ENTRAINMENT

Mold slag can be entrained into the solidifying shell due to vortexing, high velocity flow that shears slag from the surface, and turbulence at the meniscus. The capture of large inclusions into the solidifying shell then leads to obvious line defects or “slivers” in the final product.

Vortexing most often occurs during conditions of asymmetrical flow, where steel flows rapidly through the narrow passage between the SEN and the mold. This creates swirling just beside the SEN, as shown in **Fig. 19** <sup>[25]</sup>. This swirl or vortex may draw mold slag downward, near the sides of the nozzle. If it is then entrained with the jets exiting the nozzle ports, this slag will be dispersed everywhere and create defects as discussed in in the previous section. In addition to drawing in slag, the vortex is detrimental because it hastens erosion of the nozzle refractory walls. Visible erosion patterns at the locations near the off-corner and center of the wide thin-slab nozzle have been observed in practice. In addition to the vortex, slag may also be drawn downward by the recirculation pattern which accompanies flow from the nozzle ports. Thus, slag entrainment is most likely with shallow nozzle submergence and high casting speed.

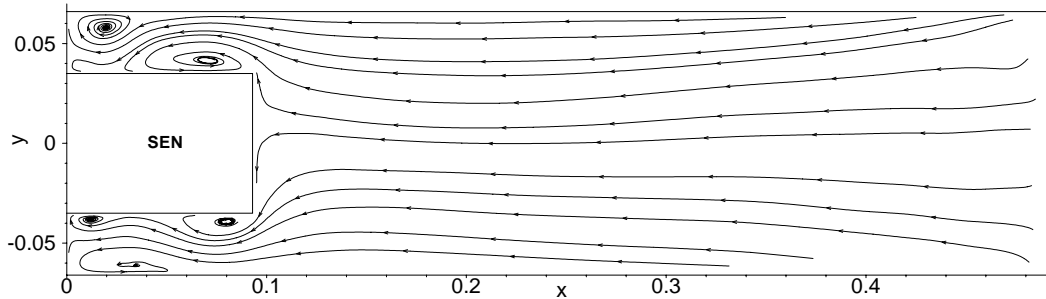


**Fig. 19** Velocity streamlines showing vortexing near SEN (in-plane 38.5 mm below top surface, flow conditions in Fig. 3) <sup>[25]</sup>

The entrainment of mold slag also occurs when the velocity across the top surface becomes high enough to shear mold slag fingers down into the flow, where they can be entrained. **Figure 20** illustrates this mechanism <sup>[12]</sup>. Once it has broken up into particles and been dispersed into the flow, the slag particles behave the same as inclusions that have entered through the nozzle. Many of these slag particles float quickly back into the slag layer, owing to their large buoyancy. However, many become entrapped as internal inclusion defects. Entrainment is easier for deeper slag layers, lower slag viscosity, and lower slag surface tension <sup>[35]</sup>. To avoid shearing slag in this manner, the top surface velocity must be kept below a critical maximum value, suggested to be 0.3 m/s or 0.4 m/s <sup>[36]</sup>. The critical velocity may also be exceeded when the standing wave becomes too severe and the interface emulsifies <sup>[37]</sup>. The critical velocity also depends on the relative densities of the steel and flux phases and the mold geometry <sup>[37]</sup>.

High velocity surface flows also may cause emulsification of the slag, where slag and steel intermix and even create a foam, if too much argon gas is present <sup>[38]</sup>. This allows easy capture of particles via vortexing or surface shearing flow. Meniscus turbulence related to level variations is another mechanism for slag entrainment, as discussed previously.

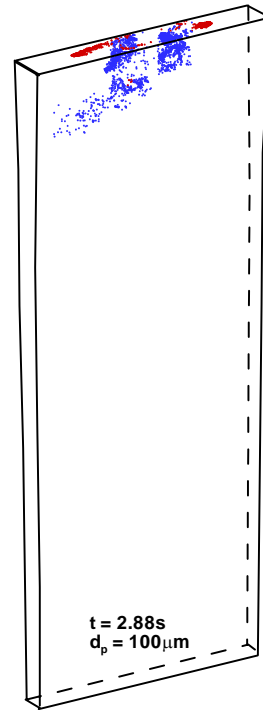


**Fig. 20.** Instantaneous snapshot of the distribution of 100  $\mu\text{m}$  slag particles, just after entrainment into the top surface (red indicates particles that refloated, while blue indicates particles that are still moving, flow conditions in Fig. 3)

## CONCLUSIONS

Fluid flow in the continuous casting process can generate many different types of defects in the final product. Computational models of fluid flow coupled with other important phenomena can be useful tools to study and quantify these problems. Several different examples of insights into defects are presented here, based on simulations conducted at the University of Illinois. These include air aspiration into the nozzle, shell thinning and breakouts from excessive superheat, surface defects from a steep "standing wave", level fluctuations, subsurface hook formation and the associated deep oscillation marks and particle entrapment, and the entrapment into the solidifying shell of inclusion particles and bubbles entering the nozzle or from mold slag entrainment at the top surface.

## ACKNOWLEDGMENTS

The author wishes to thank his former students, especially Q. Yuan, B. Zhao, and H. Shin, and Research Scientist L. Zhang for their efforts generating the results which are sampled in this paper. This work was supported by the National Science Foundation (Grant # DMI-01-15486) and the Continuous Casting Consortium at the University of Illinois. Thanks are also given to the National Center for Supercomputing Applications at the University of Illinois for computing time.

## REFERENCES

1. B.G. Thomas, "Chapter 14. Fluid Flow in the Mold," in Making, Shaping and Treating of Steel: Continuous Casting, Vol. 5, A. Cramb, ed. AISE Steel Foundation, Pittsburgh, PA, 2003, 14.1-14.41.
2. B.G. Thomas, A. Moitra and R. McDavid, "Simulation of Longitudinal Off-Corner Depressions in Continuously-Cast Steel Slabs," ISS Transactions, Vol. 23 (4), 1996, 57-70.
3. Q. Yuan, B.G. Thomas and S.P. Vanka, "Study of Transient Flow and Particle Transport during Continuous Casting of Steel Slabs, Part 1. Fluid Flow," Metal. & Material Trans. B., Vol. 35B (4), 2004, 685-702.
4. Q. Yuan, B.G. Thomas and S.P. Vanka, "Study of Transient Flow and Particle Transport during Continuous Casting of Steel Slabs, Part 2. Particle Transport," Metal. & Material Trans. B., Vol. 35B (4), 2004, 703-714.
5. B.G. Thomas, Q. Yuan, S. Sivaramakrishnan, T. Shi, S.P. Vanka, M.B. Assar, "Comparison of Four Methods to Evaluate Fluid Velocities in a Continuous Casting Mold," ISIJ Internat., Vol. 41 (10), 2001, 1266-1276.
6. Q. Yuan, B. Zhao, S.P. Vanka, B.G. Thomas, "Study of Computational Issues in Simulation of Transient Flow in Continuous Casting," Steel Research International, Vol. 76 (1), 2005, 33-43.
7. Y. Meng and B.G. Thomas, "Heat Transfer and Solidification Model of Continuous Slab Casting: CON1D," Metal. & Material Trans., Vol. 34B (5), 2003, 685-705.
8. Q. Yuan, "Transient Study of Turbulent Flow and Particle Transport During Continuous Casting of Steel Slabs," PhD Thesis, University of Illinois at Urbana-Champaign, IL, 2004.
9. B.G. Thomas and L. Zhang, "Review: Mathematical Modeling of Fluid Flow in Continuous Casting," ISIJ Internat., Vol. 41 (10), 2001, 1181-1193.
10. Q. Yuan, S. Sivaramakrishnan, S.P. Vanka, B.G. Thomas, "Computational and Experimental Study of Turbulent Flow in a 0.4-Scale Water Model of a Continuous Steel Caster," Metall. & Mater. Trans., Vol. 35B (5), 2004, 967-982.
11. B.G. Thomas, R.J. O'Malley and D.T. Stone, "Measurement of temperature, solidification, and microstructure in a continuous cast thin slab," Modeling of Casting, Welding, and Advanced Solidification Processes, (San Diego, CA), TMS, Warrendale, PA, Vol. VIII, 1998, 1185-1199.
12. Q. Yuan and B.G. Thomas, "Transport and Entrapment of Particles in Continuous Casting of Steel," 3rd International Congress on Science and Technology of Steelmaking, (Charlotte, NC, May 9-12, 2005), 2005.
13. H. Bai and B.G. Thomas, "Turbulent Flow of Liquid Steel and Argon Bubbles in Slide-Gate Tundish Nozzles, Part I, Model Development and Validation," Metall. Mater. Trans. B., Vol. 32B (2), 2001, 253-267.
14. H. Bai and B.G. Thomas, "Turbulent Flow of Liquid Steel and Argon Bubbles in Slide-Gate Tundish Nozzles, Part II, Effect of Operation Conditions and Nozzle Design," Metall. Mater. Trans. B., Vol. 32B (2), 2001, 269-284.
15. H. Bai and B.G. Thomas, "Effects of Clogging, Argon Injection and Continuous Casting Conditions on Flow and Air Aspiration in Submerged Entry Nozzles," Metall. Mater. Trans. B., Vol. 32B (4), 2001, 707-722.
16. B.G. Thomas, X. Huang and R.C. Sussman, "Simulation of Argon Gas Flow Effects in a Continuous Slab Caster," Metall. Trans. B., Vol. 25B (4), 1994, 527-547.
17. T. Shi, "Effect of argon injection on fluid flow and heat transfer in the continuous slab casting mold," MS Thesis, University of Illinois at Urbana-Champaign, 2001.
18. X. Huang, B.G. Thomas and F.M. Najjar, "Modeling Superheat Removal during Continuous Casting of Steel Slabs," Metall. Trans. B., Vol. 23B (6), 1992, 339-356.
19. Y. Meng and B.G. Thomas, "Interfacial Friction-Related Phenomena in Continuous Casting with Mold Slags," Metall. & Materials Trans. B., Vol. 34B (5), 2003, 707-725.
20. X. Huang and B.G. Thomas, "Intermixing Model of Continuous Casting During a Grade Transition," Metall. Trans. B., Vol. 27B (4), 1996, 617-632.



21. B.G. Thomas, "Modeling Study of Intermixing in Tundish and Strand during a Continuous-Casting Grade Transition," Iron and Steelmaker, Vol. 24 (12), 1997, 83-96.
22. R.C. Sussman, M. Burns, X. Huang, B.G. Thomas, "Inclusion Particle Behavior in a Continuous Slab Casting Mold," Iron & Steelmaker, Vol. 20 (2), 1993, 14-16.
23. H. Bai, "Argon Bubble Behavior in Slide-Gate Tundish Nozzles During Continuous Casting of Steel Slabs," PhD Thesis, University of Illinois at Urbana-Champaign, 2000.
24. G.D. Lawson, S.C. Sander, W.H. Emling, A. Moitra, B.G. Thomas, "Prevention of Shell Thinning Breakouts Associated with Widening Width Changes," in Steelmaking Conf. Proc., Vol. 77, ISS, Warrendale, PA, (Chicago, IL), 1994, 329-336.
25. B. Zhao, "Numerical Study of Heat Transfer in Continuous Casting of Steel," MS Thesis, University of Illinois at Urbana-Champaign, 2003.
26. B.G. Thomas, R. O'Malley, T. Shi, Y. Meng, D. Creech, D. Stone, "Validation of Fluid Flow and Solidification Simulation of a Continuous Thin Slab Caster," in Modeling of Casting, Welding, and Advanced Solidification Processes, Vol. IX, Shaker Verlag GmbH, Aachen, Germany, (Aachen, Germany, August 20-25, 2000), 2000, 769-776.
27. Q. Yuan, B.G. Thomas and S.P. Vanka, "Turbulent Flow and Particle Motion in Continuous Slab-Casting Molds," in ISSTech 2003 Process Technology Proceedings, Vol. 86, ISS, Warrendale, PA, (Indianapolis, IN, Apr 27-30, 2003), 2003, 913-927.
28. B.G. Thomas, M. Jenkins and R.B. Mahapatra, "Investigation of Strand Surface Defects Using Mold Instrumentation and Modeling," Ironmaking & Steelmaking, Vol. 31, 2004, 485-494.
29. B.G. Thomas and H. Zhu, "Thermal Distortion of Solidifying Shell in Continuous Casting of Steel," in Proceedings of International Symposia on Advanced Materials & Tech. for 21st Century, I. Ohnaka and D. Stefanescu, eds., TMS, Warrendale, PA, (Honolulu, HI), 1996, 197-208.
30. T. Honeyands and J. Herbertson, "Flow Dynamics in Thin Slab Caster Moulds," Steel Research, Vol. 66 (7), 1995, 287-293.
31. H.-J. Shin, G.G. Lee, W.Y. Choi, S.M. Kang, J.H. Park, S.H. Kim, B.G. Thomas, "Effect of Mold Oscillation on Powder Consumption and Hook Formation in Ultra Low Carbon Steel Slabs," AISTech 2004, (Nashville, TN), Assoc. Iron Steel Technology, 2004.
32. H.-J. Shin, B.G. Thomas, G.G. Lee, J.M. Park, C.H. Lee, S.H. Kim, "Analysis of Hook Formation Mechanism in Ultra Low Carbon Steel using CON1D Heat Flow - Solidification Model," Materials Science & Technology 2004, (New Orleans, LA), TMS, Warrendale, PA, Vol. II, 2004, 11-26.
33. L. Zhang, J. Sengupta and B.G. Thomas, "Investigation of Meniscus Hook Formation using Computational Models for Postech," Report, University of Illinois, 2004.
34. G. Abbel, W. Damen, G. de Gendt, W. Tiekink, "Argon Bubbles in Slabs," ISIJ Internat., Vol. 36, 1996, S219-S222.
35. J.M. Harman and A.W. Cramb, "A Study of the Effect of Fluid Physical Properties upon Droplet Emulsification," in Steelmaking Conf. Proc., Vol. 79, ISS, Warrendale, PA, (Dallas, TX), 1996, 773-784.
36. J. Kubota, K. Okimoto, A. Shirayama, H. Murakami, "Meniscus Flow Control in the Mold by Travelling Magnetic Field for High Speed Slab Caster," in Steelmaking Conference Proceedings, Vol. 74, Iron and Steel Society, (Warrendale, PA), 1991, 233-241.
37. A. Theodorakakos and G. Bergeles, "Numerical Investigation of the Interface in a Continuous Steel Casting Mold Water Model," Metall. Mater. Trans. B, Vol. 29B (6), 1998, 1321-1327.
38. W.H. Emling, T.A. Waugaman, S.L. Feldbauer, A.W. Cramb, "Subsurface Mold Slag Entrainment in Ultra-Low Carbon Steels," in Steelmaking Conf. Proc., Vol. 77, ISS, Warrendale, PA, (Chicago, IL), 1994, 371-379.